J. Plasma Physics (2001), *vol.* 66, *part* 4, *pp.* 239–257.
DOI: 10.1017/S0022377801001398 Printed in the United Kingdom

A general theory of self-similar expansion waves in magnetohydrodynamic flows

M. G. G. T. TAYLOR and P. J. CARGILL

Space and Atmospheric Physics, The Blackett Laboratory, Imperial College, London SW7 2BW, UK

(Received 2 June 2000 and in revised form 12 December 2000)

Abstract. The general theory of self-similar magnetohydrodynamic (MHD) expansion waves is presented. Building on the familiar hydrodynamic results, a complete range of possible field–flow and wave-mode orientations are explored. When the magnetic field and flow are parallel, only the fast-mode wave can undergo an expansion to vacuum conditions: the self-similar slow-mode wave has a density that increases monotonically. For fast-mode waves with the field at an arbitrary angle with respect to the flow, the MHD equations have a critical point. There is a unique solution that passes through the critical point that has $\frac{1}{2}\gamma\beta = 1$ and $B_r = 0$ there, where γ is the polytropic index, β the local plasma beta and B_r the radial component of the magnetic field. The critical point is an umbilical point, where sound and Alfvén speeds are equal, and the transcritical solution undergoes a change from a fast-mode to a slow-mode expansion at the critical point. Slow-mode expansions exist for field-flow orientations where the angle between field and flow lies either between 90° and 180° or between 270° and 360°. There is also an umbilic point in these solutions when the initial plasma beta β_0 exceeds a critical value $\beta_{\rm crit}$. When $\beta_0 \geqslant \beta_{\rm crit}$, the solutions require a transition through a critical point. When $\beta_0 < \beta_{\rm crit}$, there is a smooth solution involving an inflection in the density and angular velocity. For other angles between field and flow, all the slow-mode waves are compressive. An analytic solution for the case of a magnetic field everywhere perpendicular to the flow with $\gamma = 2$ is presented.

1. Introduction

The problem of how a supersonic fluid interacts with corners is one of longstanding interest in many areas of fluid dynamics and aerodynamics. The solution to the problem was identified in 1903 by Prandtl and Meyer, who recognised that a series of expansion waves would originate at the corner, and accelerate and rarefy the flow as it moved around the corner. Analytical solutions are possible if the flow is assumed to be self-similar – that is to say the flow properties are independent of the radial distance from the corner, and depend only on the angular distance from the start of the expansion wave. These solutions are well documented in most textbooks on gas dynamics (e.g. Landau and Lifschitz 1988; Curle and Davies 1971). An important point is that the flow reaches a vacuum condition after a finite rotation.

The situation is more complex in a magnetised fluid. There are two possible expansive wave modes of interest – the fast and slow magnetohydrodynamic (MHD)

waves – both of which are more complex that the pure acoustic wave that determines the behaviour in the gas-dynamic case. Additional parameters are the plasma beta (ratio of gas to magnetic pressure), relative orientation of field and flow, and equation of state. No systematic study of such waves has been carried out. Siscoe et al. (1969) made some progress by obtaining expressions for the characteristic flow speeds, but only presented solutions of the MHD equations in the hypersonic limit. Goedbloed and Lifshitz (1997) have presented an extensive analysis of self-similar MHD flows, concentrating on cases when the flow and magnetic field are aligned with each other (i.e. where there is no electric field). Very specific applications have also appeared in the literature (see below) over the years, but without a general theoretical framework being provided.

MHD expansion waves are important structures in many areas of space plasma physics, particularly when high-speed flows interact with abrupt changes in the Earth's magnetic field strength or topology (Siscoe and Sanchez 1986; Cargill 1999) or with other (unmagnetised) obstacles such as moons (Siscoe et al. 1969; Krisko and Hill 1991) or asteroids. Siscoe and Sanchez (1986) presented some solutions of a slow-mode expansion wave in the Earth's magnetotail, and showed that such a wave was an integral part of the expansion of the shocked solar wind into the Earth's magnetotail. Cargill (1999) argued that the interaction of a supersonic solar wind flow with the Earth's cusp would be accomplished through an expansion wave, and noted that plasma could not move significantly Earthward during this interaction. Siscoe et al. (1969) investigated the interaction of a hypersonic flow with the Moon, and noted that fast-mode expansion waves played a major role here, whereas Krisko and Hill (1991) investigated slow-mode expansion waves in the low-plasma-beta environment of the Jovian moon Io.

While investigating plasma flows in the magnetospheric cusp, it became apparent that there is no theory that describes such MHD expansion waves in *general* terms. That is the purpose of this paper. Section 2 describes briefly the basic hydrodynamic theory of self-similar expansion waves. Section 3 derives the appropriate MHD equations, and describes some important properties. Section 4 presents the main results of the paper for different field–flow orientations, and for both fast and slow wave modes and also contains a useful analytical solution that has been used to benchmark numerical solutions of the MHD equations.

2. Basic concepts and hydrodynamic theory

The ideal, steady-state, MHD equations are

$$\boldsymbol{\nabla} \cdot (\rho \mathbf{V}) = 0, \tag{1}$$

$$\rho(\mathbf{V} \cdot \boldsymbol{\nabla})\mathbf{V} = -\boldsymbol{\nabla} P + \mathbf{j} \times \mathbf{B}, \tag{2}$$

$$\boldsymbol{\nabla} \times (\mathbf{V} \times \mathbf{B}) = 0, \tag{3}$$

$$\boldsymbol{\nabla} \cdot \mathbf{B} = 0, \tag{4}$$

$$\frac{d}{dt}\left(\frac{P}{\rho^{\gamma}}\right) = 0, \tag{5}$$

where ρ, P, $\mathbf{V}$ and $\mathbf{B}$ are the plasma density, pressure, velocity and magnetic field respectively, and we have assumed an adiabatic relationship between density and pressure, with γ the ratio of specific heats.

https://doi.org/10.1017/S0022377801001398 Published online by Cambridge University Press

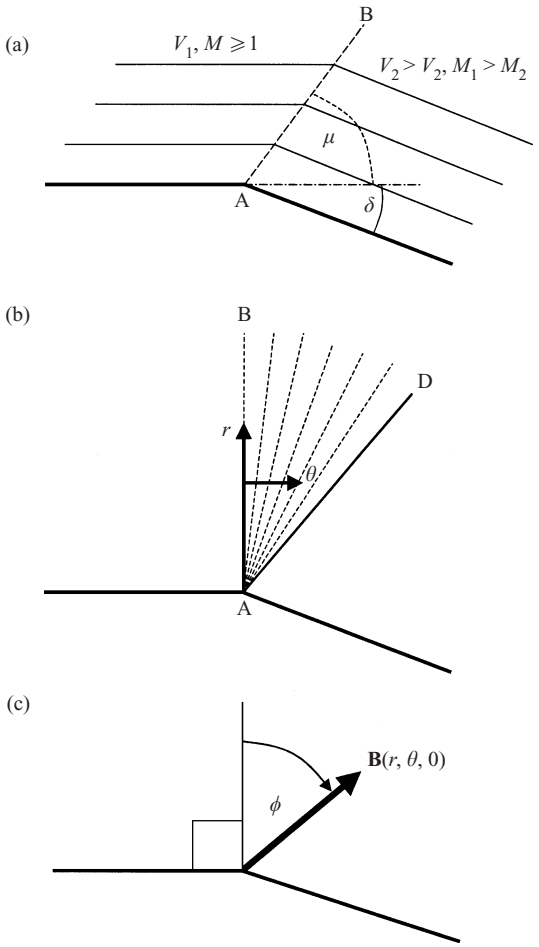

Figure 1. A sketch of the geometry used in the expansion-wave model. (a) shows a supersonic fluid moving from left to right along a surface (thick lower lines). At point A, there is a corner, where the surface turns through an angle δ. A Mach line is shown (line AB), making an angle of $\mu = \sin^{-1}(1/M)$ with respect to the upstream flow, where M is the Mach number. The thin lines represent streamlines. (b) shows the structure of the expansion fan. It extends in the angular direction between the lines AB and AD. (c) defines the angle ϕ between the initial undisturbed flow and the magnetic field in the (r, θ) plane. In all the results, we assume that the initial flow has a Mach number (based on the relevant wave speed) of unity (see text).

The geometry with which we are concerned here is shown in Fig. 1(a). A steady-state supersonic flow is directed from left to right along a boundary (thick line). At point A, the boundary turns through an angle δ. The issue at hand is how the flow behaves at the corner. (We note here that the abrupt change in the boundary can be taken as a model for a more gradual corner (Curle and Davies 1971).) In an unmagnetised fluid (e.g. a gas such as air), the corner acts as a source of sound waves. The supersonic flow has no forewarning of the corner, since these waves cannot propagate upstream and so the flow first 'knows' about the corner when it encounters the first Mach line (line AB in Fig. 1), which makes an angle of $\mu = \sin^{-1}(1/M)$ with respect to the upstream flow, where M is the Mach number. From this point onward, the corner influences the flow, with the flow being turned

https://doi.org/10.1017/S0022377801001398 Published online by Cambridge University Press

around the corner by a continuous series of expansion waves (often referred to as an expansion fan) as shown in Fig. 1(b) (see also Curle and Davies 1971, pp. 119–120).

For many situations, the flow around such a corner is self-similar. To formalise this, we define a cylindrical coordinate system (r, θ, z), with the origin at point A in Fig. 1(a) and θ increasing in the clockwise direction. z completes the orthogonal system, being directed into the paper. It can be seen from Fig. 1(b) that while the width of the wave or fan increases with r, the overall structure is the same at all values of r. This leads to a great simplification in the equations of fluid dynamics (and MHD: Sec. 3), since all derivatives with respect to r can be discarded. (We also assume invariance in the z direction.) Figure 1(c) shows the nomenclature for the magnetic field direction in the (r, θ) plane ($B_z = 0$), to be used in Sec. 4.3.

The theory of such a flow is well known (see e.g. Curle and Davies 1971; Cargill 1999) and need only be restated briefly here. We take the fluid limit of (1)–(5), i.e. $B = 0$, and write the surviving equations in cylindrical coordinates:

$$V_r \frac{\partial V_r}{\partial r} + \frac{V_\theta}{r}\frac{\partial V_r}{\partial \theta} - \frac{V_\theta^2}{r} = -\frac{1}{\rho}\frac{\partial P}{\partial r}, \tag{6}$$

$$V_r \frac{\partial V_\theta}{\partial r} + \frac{V_\theta}{r}\frac{\partial V_\theta}{\partial \theta} + \frac{V_\theta V_r}{r} = -\frac{1}{r\rho}\frac{\partial P}{\partial \theta}, \tag{7}$$

$$\rho\left(\frac{V_r}{r} + \frac{\partial V_r}{\partial r}\right) + \rho\left(\frac{1}{r}\frac{\partial V_\theta}{\partial \theta}\right) + V_r\frac{\partial \rho}{\partial r} + \frac{V_\theta}{r}\frac{\partial \rho}{\partial \theta} = 0. \tag{8}$$

Equations (6)–(8) are the r and θ components of the momentum equation and the continuity equation respectively. One may also derive Bernoulli's equation along a streamline:

$$\tfrac{1}{2}V^2 + \frac{\gamma}{\gamma - 1}\frac{P}{\rho} = X_1, \tag{9}$$

where X_1 is constant along a streamline, and can be defined in terms of quantities at some point in the undisturbed fluid, denoted by subscript zero. Hence,

$$X_1 = \tfrac{1}{2}V_0^2 + \frac{\gamma}{\gamma - 1}\frac{P_0}{\rho_0}.$$

In the absence of a magnetic field, (6)–(8) can be combined to give

$$\left(1 - \frac{C^2}{V_\theta^2}\right)\left(\frac{dV_\theta}{d\theta} + V_r\right) = 0, \tag{10}$$

where $C^2 = \gamma P/\rho$ is the square of the sound speed, with P and ρ being the pressure and density respectively and γ the polytropic index. Equation (10) has two solutions. Setting the second factor to zero gives a trivial (constant pressure) solution. Therefore the only physically interesting solution to (10) is

$$V_\theta = \pm C, \tag{11}$$

so that the velocity in the θ direction is just the *local* sound speed. Taking the positive root in (11), analytic expressions can then be obtained for the radial flow

https://doi.org/10.1017/S0022377801001398 Published online by Cambridge University Press

V_r and the local Mach number $M^2 = V^2/C^2$ as follows:

$$V_r = \left\{ 2X_1 \sin\left[\left(\frac{\gamma - 1}{\gamma + 1} \right)^{1/2} \theta \right] \right\}^{1/2}, \tag{12}$$

$$M^2 = \frac{V_r^2 + V_\theta^2}{C^2} = \frac{V_r^2}{V_\theta^2} + 1 = \left(\frac{\gamma + 1}{\gamma - 1} \right) \tan^2 \left[\left(\frac{\gamma + 1}{\gamma - 1} \right)^{1/2} \theta \right] + 1, \tag{13}$$

where $V_r = 0$ at $\theta = 0$ and X_1 is the constant from the Bernoulli equation. Solutions for expanding flows can then be constructed in the following way. Equations (12) and (13) represent the expansion of an $M = 1$ flow. For a supersonic flow incident on a corner with $M > 1$, one simply matches the appropriate solution of an $M = 1$ expansion, given by (12) and (13), to the incident flow at the first Mach line (AD in Fig. 1). This gives the Prandtl–Meyer function:

$$\nu = \left(\frac{\gamma + 1}{\gamma - 1} \right)^{1/2} \tan^{-1} \left[\left(\frac{\gamma - 1}{\gamma + 1} \right)^{1/2} (M^2 - 1)^{1/2} \right] - \tan^{-1}[(M^2 - 1)^{1/2}],$$

where ν is the Prandtl–Meyer angle, defined as the angle turned by the superposed $M = 1$ flow to the final edge of the fan at AD. As mentioned previously, a thorough description of this Prandtl–Meyer expansion fan analysis is readily available in the literature (see e.g. Curle and Davies 1971, pp. 122–123). Note that the density vanishes (i.e. a vacuum condition is attained) at a finite value of θ.

3. MHD equations for self-similar expansive flows

It is straightforward to write down the MHD equations for a self-similar flow. We assume a general magnetic field of the form: $\mathbf{B} = (B_r(\theta), B_\theta(\theta), B_z(\theta))$, and a plasma flow in the (r, θ) plane: $\mathbf{V} = (V_r(\theta), V_\theta(\theta), 0)$. The solenoidal condition (4) then becomes

$$\frac{dB_\theta}{d\theta} + B_r = 0. \tag{14}$$

From the z component of the momentum equation, we have

$$B_\theta \frac{dB_z}{d\theta} = 0, \tag{15}$$

so that if $B_\theta \neq 0$ then $B_z = \text{const}$. In general, we set $B_z = 0$ for simplicity. (The case $B_\theta = 0$, $B_z \neq 0$ requires separate treatment (see Sec. 4.1).) The mass-continuity equation remains unchanged from the fluid case, and is

$$\rho V_r + \frac{d}{d\theta}(\rho V_\theta) = V_\theta \frac{d\rho}{d\theta} + \rho \left(V_r + \frac{dV_\theta}{d\theta} \right) = 0. \tag{16}$$

The r and θ components of the momentum equation are

$$\rho V_\theta \left(\frac{dV_r}{d\theta} - V_\theta \right) = \frac{B_\theta}{\mu_0} \left(\frac{dB_r}{d\theta} - B_\theta \right), \tag{17}$$

$$\rho V_\theta \left(\frac{dV_r}{d\theta} + V_r \right) = -\frac{d}{d\theta} \left(p + \frac{B^2}{2\mu_0} \right) + \frac{B_\theta B_r}{\mu_0} + \frac{B_\theta}{\mu_0} \frac{dB_\theta}{d\theta} \tag{18}$$

Finally, combining Faraday's law with Ohm's law for a perfect conductor gives

https://doi.org/10.1017/S0022377801001398 Published online by Cambridge University Press

the condition

$$\frac{d}{d\theta}(V_r B_\theta - V_\theta B_r) = 0, \tag{19}$$

such that E_z = const. Following Siscoe et al. (1969), we combine these equations to obtain

$$\left[\left(\rho V_\theta^2 - \frac{B_\theta^2}{\mu_0}\right)(\rho V_\theta^2 - \gamma p) - \rho V_\theta^2 \frac{B_r^2}{\mu_0}\right]\left(\frac{dV_\theta}{d\theta} + V_r\right) = 0, \tag{20}$$

where a polytropic law $p = a\rho^\gamma$ has been used. As in the hydrodynamic case, setting the second factor to zero gives a physically trivial solution. Setting the first factor to zero gives the following expression for V_θ:

$$V_\theta^2 = \tfrac{1}{2}\{C_s^2 + V_A^2 \pm [(C_s^2 + V_A^2)^2 - 4C_s^2 V_{A\theta}^3]^{1/2}\}, \tag{21}$$

the solutions of which correspond to θ flows at either the local fast or slow-mode speeds. In (21), $V_A = |B|/(\mu_0\rho)^{1/2}$ and $V_{A\theta} = B_\theta/(\mu_0\rho)^{1/2}$ are the Alfvén speeds based on the total and angular field strengths respectively.

To proceed further, we write the equations in dimensionless units. All quantities are normalised with respect to values at $\theta = 0$, denoted here by the subscript 0. Thus, in (14)–(21), we replace ρ by ρ/ρ_0, B by B/B_0, V by V/C_0, etc. For clarity, we do not introduce new symbols for these dimensionless physical quantities. Equation (21) then becomes

$$V_\theta^2 = \tfrac{1}{2}\left\{\rho^{\gamma-1} + \frac{2B^2}{\gamma B_0 \rho} \pm \left[\left(\rho^{\gamma-1} + \frac{2B^2}{\gamma\beta_0\rho}\right)^2 - \frac{8\rho^{\gamma-2}B_\theta^2}{\gamma\beta_0}\right]^{1/2}\right\}, \tag{22}$$

where $\beta_0 = 2\mu_0 p_0/B_0^2$ is the plasma beta at $\theta = 0$. Equations (14) and (20) are

$$\frac{dB_\theta}{d\theta} = -B_r \tag{23}$$

$$\frac{dB_r}{d\theta} = B_\theta - \frac{\dfrac{B_r M_{A\theta}^2}{V_\theta}\left(V_r + \dfrac{dV_\theta}{d\theta}\right)}{M_{A\theta}^2 - 1}. \tag{24}$$

Finally, the continuity equation and the radial momentum equation are written in the following form (where (24) has been used in the derivation of (26)):

$$\frac{d\rho}{d\theta} = -\frac{-\rho V_r - \rho\dfrac{dV_\theta}{d\theta}}{B_\theta}, \tag{25}$$

$$\frac{dV_r}{d\theta} = V_\theta - \frac{\dfrac{2B_\theta B_r M_{A\theta}^2}{\gamma\rho\beta_0 V_\theta^2}\left(V_r + \dfrac{dV_\theta}{d\theta}\right)}{M_{A\theta}^2 - 1}. \tag{26}$$

Note that we do not require the θ component of the momentum equation. All information therein is contained in the other equations (including (22)). An important value in these equations is $M_{A\theta}$, the Alfven Mach number based on the θ components of field and flow:

$$M_{A\theta} = \frac{V_\theta}{V_{A\theta}}. \tag{27}$$

We note here that both (24) and (26) possess critical points when $M_{A\theta} = 1$ and

https://doi.org/10.1017/S0022377801001398 Published online by Cambridge University Press

$B_r = 0$. This will be of importance in understanding our results. Equations (22)–(26) form a set of five equations for five variables, and are solved numerically using a fourth-order Runge–Kutta scheme with appropriate initial conditions at $\theta = 0$.

4. Results

4.1. Field perpendicular to flow

In Sec. 3, it was shown from (15) that when there is a field component in the plane of the flow, B_z must be constant. However, if $B_r = B_\theta = 0$, this condition no longer holds, and one can solve the MHD equations for a variable B_z. This type of flow is not described by (22)–(26), which have explicitly set $B_z = 0$. From the induction equation (3), we may write

$$\frac{d}{d\theta}(V_\theta B_z) = -V_r B_z. \tag{28}$$

For $\mathbf{B} = (0, 0, B_z(\theta))$, and $\mathbf{V} = (V_r(\theta), V_\theta(\theta), 0)$, (14) and (15) are satisfied. We can combine (28) with (16) such that

$$\frac{B}{\rho} = \text{const}, \tag{29}$$

and so $B/B_0 = \rho/\rho_0$. In this case, we find that $V_\theta^2 = C^2 + V_A^2$, so that the angular velocity is now the fast-mode speed. One can obtain a Bernoulli equation for the flow along a streamline:

$$\tfrac{1}{2}V^2 + \frac{\gamma}{\gamma - 1}\frac{P}{\rho} + V_A^2 = X_2, \tag{30}$$

where X_2 is a constant of integration written in terms of the upstream conditions. Equation (30) can be written as

$$V_r^2 = X_2 - \frac{\gamma + 1}{\gamma - 1}C^2 - 3V_A^2. \tag{31}$$

We note that as $B/B_\infty = \rho/\rho_\infty$, V_θ and V_r can be described completely in terms of density. For this magnetic field orientation, we have $dV_r/d\theta = V_\theta$, and so obtain the following expression for V_r:

$$\int \frac{dV_r}{\left(2X_2 - V_r^2 + 2V_A^2\dfrac{\gamma - 2}{\gamma - 1}\right)^{1/2}} = \int \left(\frac{\gamma - 1}{\gamma + 1}\right)^{1/2} d\theta. \tag{32}$$

Unlike the hydrodynamic case, in general the integral on the left-hand side cannot be evaluated analytically. For the special case of a polytropic index $\gamma = 2$, analytical solutions are possible. These analytical results are presented below, and have been used as a test of our numerical integration scheme. We find

$$V_r = \left[3\left(\frac{\beta_0 + 1}{\beta_0}\right)\sin\left(\frac{\theta}{\sqrt{3}}\right)\right]^{1/2}, \tag{33}$$

and an expression for the density

$$\rho = \cos^2\left(\frac{\theta}{\sqrt{3}}\right), \tag{34}$$

https://doi.org/10.1017/S0022377801001398 Published online by Cambridge University Press

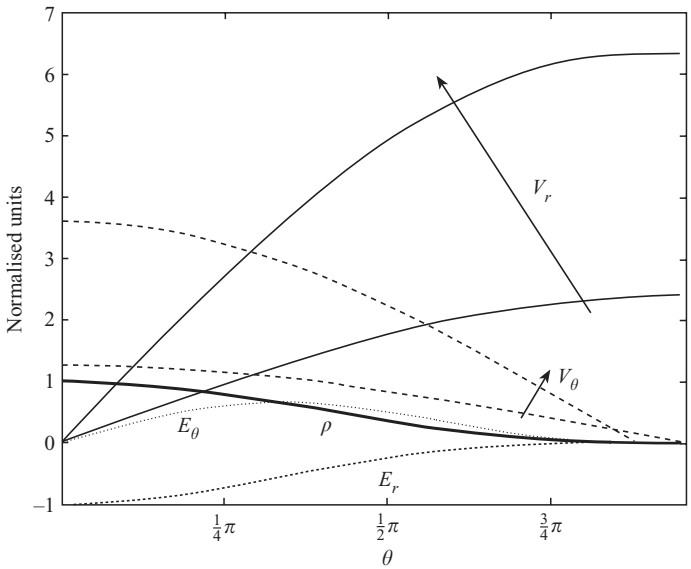

Figure 2. The structure of an MHD expansion wave when the magnetic field is directed in the z direction, and is everywhere perpendicular to the flow. The thin solid, thick solid and dashed line show V_r, ρ and V_θ respectively. We note that in all the figures, velocities, density and magnetic field are shown in dimensionless units, with the magnetic field, velocity and density in units of the magnetic field, sound speed and density at $\theta = 0$ respectively, i.e. $B = B/B_0$, $V = V/C_0$, etc. β_0 varies from 0.1 to 2, with decreasing β_0 being shown by the direction of the arrows. The density shows little change as β_0 is varied, so only one value is shown. The electric field **E** initially points in the negative r direction, and decreases through the fan to very small values.

independent of the plasma beta. This is reflected in our numerical solutions described below.

Figure 2 shows the density and radial and angular velocities as functions of θ for this case with $\gamma = \frac{5}{3}$ and β_0 ranging from 0.1 to 2. At $\theta = 0$, we have $\rho = 1$, $V_r = 0$ and $V_\theta = (1 + 2/\gamma\beta_0)^{1/2}$, so that the initial flow is exactly at the fast-mode speed. In all the figures, we show the complete expansion from $\theta = 0$ to termination at a vacuum condition: solutions for particular cases can be obtained by picking up the solution at the appropriate angle corresponding the Mach number of interest.

In this case, large values of β_0 correspond to the well-known hydrodynamic case. As β_0 decreases, we see that (i) the vacuum condition (shown by the termination of the V_θ plots) is reached for smaller values of θ, (ii) the radial velocity increases quite considerably, and (iii) the density profile is insensitive to the value of β_0. In addition, the local plasma beta is proportional to $\rho^{\gamma-2}$, so that for $\gamma < 2$, β always tends to infinity when the vacuum condition is reached, i.e. the expansion becomes purely hydrodynamic. The first two results can be understood by recognising that decreasing β_0 leads to a larger magnetic pressure force, which decelerates the angular flow more rapidly, hence leading to earlier vacuum conditions. The final result is not surprising given the analytical result in (34). In this field geometry, the electric field is given by $\mathbf{E} = (-V_\theta B_z, V_r B_z, 0)$. As mentioned previously, the velocity components can be described in terms of the density only. Because of this and the relationship between B and ρ, **E** can be defined purely in terms of the density. The

https://doi.org/10.1017/S0022377801001398 Published online by Cambridge University Press

components of **E** are shown in Fig. 2, and it is found that **E** tends to very small values as vacuum conditions are approached. At $\theta = 0$, **E** is in the negative r direction, reflecting the fact that **B** is directed out of the fiugre (from $\mathbf{E} = -\mathbf{V} \times \mathbf{B}$). We note that in the subsequent cases, $\mathbf{B} = (B_r, B_\theta, 0)$ so that the resulting electric field, $\mathbf{E} = (0, 0, E_z)$ is constant, as defined by (19).

4.2. Field parallel to the flow

The second simple case that can be considered is where the flow and field are everywhere parallel to each other. Two approaches have been attempted. In one, the MHD equations were written in terms of pseudo-variables (Grad 1960). This is discussed elsewhere (Taylor 2000). In this paper, we solve the MHD equations in their standard form. When the velocity and magnetic field are parallel, the electric field vanishes, so that (19) becomes $V_r B_\theta = V_\theta B_r$. Thus, if the flow and field are parallel at $\theta = 0$, they are parallel for all values of θ. One can then write $\mathbf{B} = \lambda\rho\mathbf{V}$ (Grad 1960), where λ is a constant, and substitute this relation into the MHD equations. The Bernoulli equation becomes

$$\frac{V^2}{2} + \frac{C^2}{\gamma - 1} = X_3 \text{ (const)}, \tag{35}$$

and one can hence derive an expression for the angular velocity:

$$V_\theta^2 = C^2 + \frac{2\lambda^2}{\mu_0}\rho X_3 - \frac{\lambda^2}{\mu_0}\frac{\gamma + 1}{\gamma - 1}\gamma p, \tag{36}$$

which appears to differ from (21). We will return to this interesting and important issue shortly. Equation (36) can be written in the more transparent form

$$V_\theta^2 = C^2 + \frac{\dfrac{2\rho}{\gamma\beta_0}V_r^2}{1 - \dfrac{2\rho}{\gamma\beta_0}}. \tag{37}$$

Since $\rho = \rho(\theta)$, we can write the continuity equation as

$$\frac{d\rho}{d\theta} = \frac{-V_r\rho}{V_\theta + \rho\dfrac{dV_\theta}{d\rho}} \tag{38}$$

and the radial momentum equation as

$$\frac{dV_r}{d\theta} = \frac{V_\theta - \dfrac{2\rho}{\gamma\beta_0}\left(V_\theta - \dfrac{V_r}{\rho}\dfrac{d\rho}{d\theta}\right)}{1 - \dfrac{2\rho}{\gamma\beta_0}}. \tag{39}$$

Note that the solenoidal condition is automatically satisfied in this case. One thus needs to solve (36)–(39) subject to appropriate conditions at $\theta = 0$. We have $V_r = 0$ there, so (37) gives $V_\theta = 1$ as the initial condition, as one finds in the hydrodynamic case. However, it should be noted that as β_0 changes from being $\gg 1$ to $\ll 1$, this initial value of V_θ changes from being a fast-mode wave to being a slow-mode wave. We now explore the consequences of this.

The results are shown in Figs 3(a) and (b), in the same format as Fig. 2. As before, $\gamma = \frac{5}{3}$ and β_0 varied from $\ll 1$ to $\gg 1$. Figures 3(a) and (b) show the results for β_0

https://doi.org/10.1017/S0022377801001398 Published online by Cambridge University Press

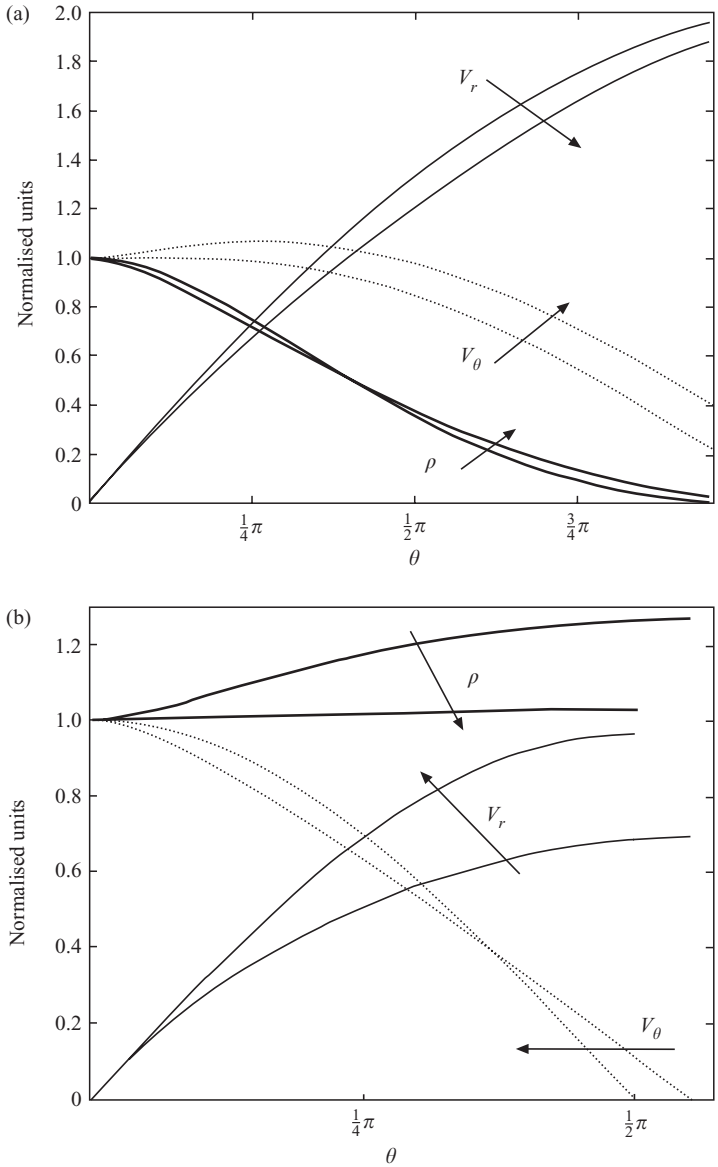

Figure 3. The wave structure when the magnetic field and plasma flow are everywhere parallel. The notation is the same as in Fig. 2. (a) and (b) show results for $\frac{1}{2}\gamma\beta_0 > 1$ and < 1 respectively, with 3(a) showing $4 > \beta_0 > 2$ and 3(b) $0.9 > \beta_0 > 0.1$. The direction of decreasing β_0 is indicated by the arrows. In (a), a fast-mode expansion wave exists, while in (b), the only possible solutions correspond to slow-mode compression waves with pressure and magnetic field strength out of phase.

between 4 and 2, and between 0.9 and 0.1 respectively. (We return to intermediate values (especially $\frac{1}{2}\gamma\beta_0 = 1$) shortly.) Figure 3(a) shows that as β_0 decreases, there is relatively little change in the properties of the expansion wave. The radial velocity decreases with decreasing β_0, a reflection of the fact that smaller β_0 imply a larger magnetic tension force, which inhibits any radial flow. Decreasing β_0 also leads to

https://doi.org/10.1017/S0022377801001398 Published online by Cambridge University Press

the vacuum condition occurring at larger angles. An important diagnostic of fast and slow MHD waves is the relative phase of the pressure and magnetic field. Fast (slow) waves have the pressure and magnetic field in (out of) phase. For the values of β_0 shown in Fig. 3(a), p and B^2 are in phase for all values of θ.

When β_0 is decreased below unity, the character of the solutions changes entirely (Fig. 3b). The only solution in this case is a compression wave, with the density increasing monotonically. We find that p and B^2 are now out of phase for all values of θ. This is thus a slow-mode wave, as was predicted above, and is compressive, suggesting that (at least for the case of field-aligned flow) self-similar expansion waves do not exist for this range of β_0. The solution is terminated when V_θ vanishes. Note also that as β_0 becomes small, the density variations become negligible. One now has a rather rigid magnetic field structure, with the flow simply being guided along it.

We now return to the apparent inconsistency between (22) and (36). For field-aligned flow, (22) gives two possible initial values of V_θ, namely 1 and $2/\gamma\beta_0$. For $\beta_0 \gg 1$ ($\ll 1$), these two values are the fast (slow) and slow (fast) waves. However, an examination of (20) shows that an initial state at $\theta = 0$, with direct substitution of $\mathbf{B} = \lambda\rho\mathbf{V}$ and $V_r = 0$, permits only a single solution. Thus, the only solutions permitted for field-aligned flow are fast-mode expansive waves for $\frac{1}{2}\gamma\beta_0 > 1$ and slow-mode compressive waves for $\frac{1}{2}\gamma\beta_0 < 1$. We note that this behaviour was also reported in Goedbloed and Lifshitz (1997).

4.3. General field–flow orientation: fast-mode waves

The above solution involves a constraint on the relation between the field and flow. However, it serves to draw attention to the rather complex nature of self-similar MHD expansion waves. We now address the general case of when the field and flow have an arbitrary angle with respect to each other. One must solve (22)–(26), subject to the appropriate boundary conditions at $\theta = 0$. To demonstrate the essential features of the solutions, we focus on a specific case where the field and flow are perpendicular to each other at $\theta = 0$. An angle ϕ is introduced to quantify this orientation. Figure 1(c) shows how ϕ is defined: the present case corresponds to $\phi = \pi$. In this case, the field has only a radial component at $\theta = 0$, so that field and flow are initially perpendicular. Thus the only possible initial state corresponds to a fast-mode expansion wave. As was noted in Sec. 3, the solution can be expected to have interesting properties at the critical point when $M_{A\theta} = 1$ and $B_r = 0$. Drawing on extensive experience with such critical points in MHD flows (see e.g. Weber and Davies 1967), one might anticipate that there is a unique initial condition that permits a continuous solution through the critical point. We define this unique initial condition as having $\beta_0 = \beta_{\rm crit}$. Figure 4 shows V_r (upper curves) and B_r (lower curves) for three values of β_0 (0.5, 1.8 and 5). For $\beta_0 = 5$, $\beta_0 > \beta_{\rm crit}$ (lower curve of V_r and B_r), the solution breaks down, with $dV_r/d\theta \to -\infty$ when $M_{A\theta} = 1$. For $\beta_0 = 0.5$, $\beta_0 < \beta_{\rm crit}$ (upper curve of V_r and B_r), the solution breaks down at a smaller value of θ, with $dV_r/d\theta \to \infty$. Note that $B_r < 0$ there. Finally, the central curves (shown as thick solid lines) have $\beta_0 = 1.8 = \beta_{\rm crit}$, and the solutions do not break down before the critical point.

We now turn to the properties of the transcritical solution. Figure 5 shows this solution over the entire range of θ. Up to the critical point, the solution corresponds to a fast-mode expansion wave with B_r, B^2 (not shown) and the density decreasing in phase with each other. Noting that $dB_\theta/d\theta$ vanishes at the critical point, (25) can

https://doi.org/10.1017/S0022377801001398 Published online by Cambridge University Press

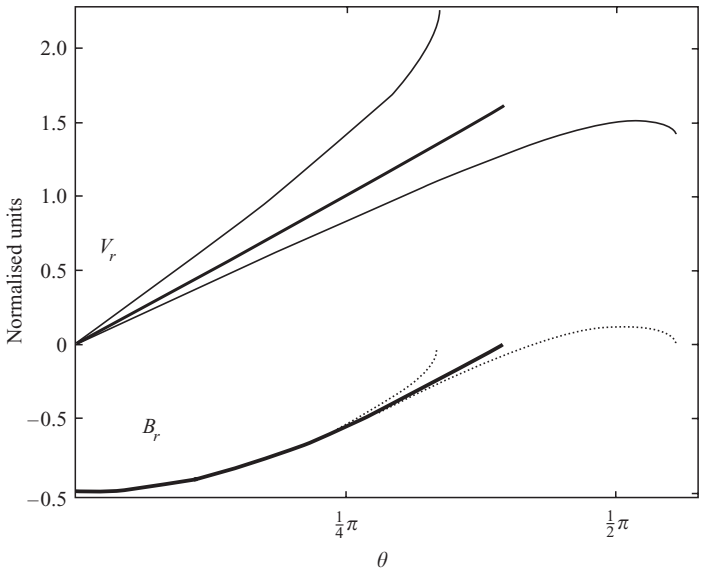

Figure 4. The expansion-wave structure for solutions to the left of the critical point. The upper and lower sets of curves show V_r and B_r respectively. Three values of β_0 are shown. From left to right, the three curves have $\frac{1}{2}\gamma\beta_0 = 0.5$, 1.8 and 5 respectively. Only the solution with $\beta_0 = 1.8$ reaches the critical point, and is shown by the thick solid lines. The other solutions all break down before the critical point is reached.

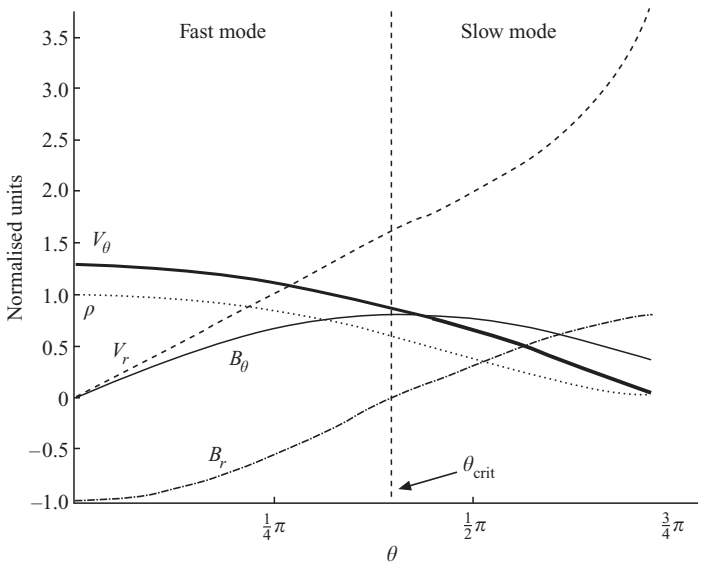

Figure 5. The solution that passes through the critical point, which has $\beta_0 = 1.8$. To the left of the critical point, the expansion wave is a fast-mode wave. To the right, it is a slow-mode wave.

only be satisfied if B_r *increases* beyond the critical point. However, in order to have an expansion solution to the right of the critical point, the density must continue to decrease, and so B_r (and B^2) and ρ are now out of phase with each other. Thus the continuous solution must be slow-mode beyond the critical point: computationally,

https://doi.org/10.1017/S0022377801001398 Published online by Cambridge University Press

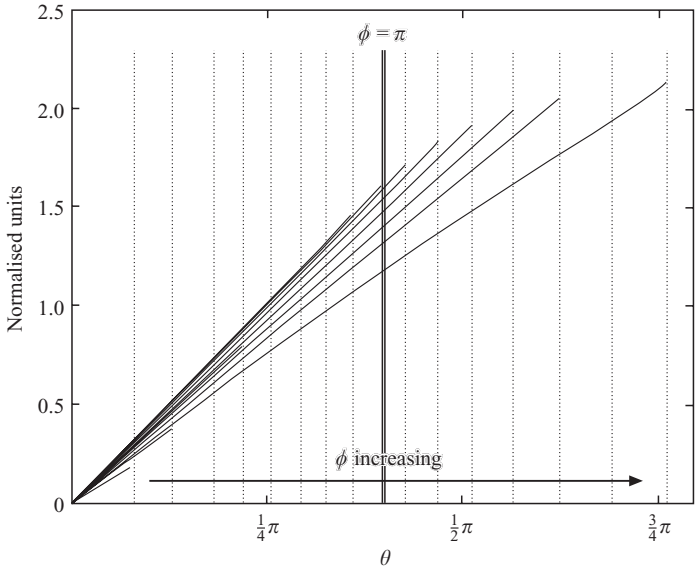

Figure 6. V_r for the critical solutions to the *left* of the critical point, as the angle ϕ is increased from $\frac{1}{2}\pi$ to $\frac{3}{2}\pi$ (see Fig. 1 for a definition of ϕ). Here $\frac{1}{2}\gamma\beta = 1$ at the critical point for each solution, and the critical point moves to the right as ϕ is increased. The cases of $\phi = \frac{1}{2}\pi$ and $\frac{3}{2}\pi$ correspond to field-aligned flow and hence do not need to pass through a critical point for $\frac{1}{2}\gamma\beta_0 > 1$, and are not shown.

this is achieved by taking the minus sign in (22). The entire solution is thus fast-mode up to the critical point, and slow-mode thereafter.

Such a transition from fast to slow mode at a critical point can only be accomplished if the relevant wave speeds are identical at the critical point. Since $B_r = 0$ there, the two solutions for V_θ are simply $V_\theta = C$ and $V_\theta = V_A$. Such a point is sometimes referred to as an umbilical point (Myong 1997). Further, if $C = V_A$, this point corresponds to a location where $\frac{1}{2}\gamma\beta = 1$, with β now the local plasma beta. In other words, when $\beta_0 = \beta_{\rm crit}$, we attain the umbilic conditions at the critical point, and thus are able to continue the expansion to vacuum conditions via the slow mode.

Figure 6 shows the transcritical solution V_r to the left of the critical point as the angle ϕ is increased from $\frac{1}{2}\pi$ to $\frac{3}{2}\pi$. The initial conditions are assumed to correspond to a fast-mode wave, since for $\phi \neq \pi$ both fast- and slow-mode waves are valid initial conditions. As ϕ approaches $\frac{1}{2}\pi$, $\frac{1}{2}\gamma\beta_0 < 1$ and so there is no expansive solution when $\phi = \frac{1}{2}\pi$ (see Sec. 4.2). When $\phi = \frac{3}{2}\pi$, the vacuum condition is reached before the critical point. As ϕ increases, the location of the umbilical point moves to increasing values of θ, so that by the time ϕ approaches $\frac{3}{2}\pi$ the critical point is located 3 radians into the expansion, and the density is very close to the vacuum condition.

4.4. General field–flow orientation: slow-mode waves

We now turn to the case of expansion waves where the wave to the left of the critical point is slow-mode. The slow-mode wave can be expected to exhibit considerable dependence on the angle ϕ. When $\phi = 0$ or π, there is no slow-mode wave. When

https://doi.org/10.1017/S0022377801001398 Published online by Cambridge University Press

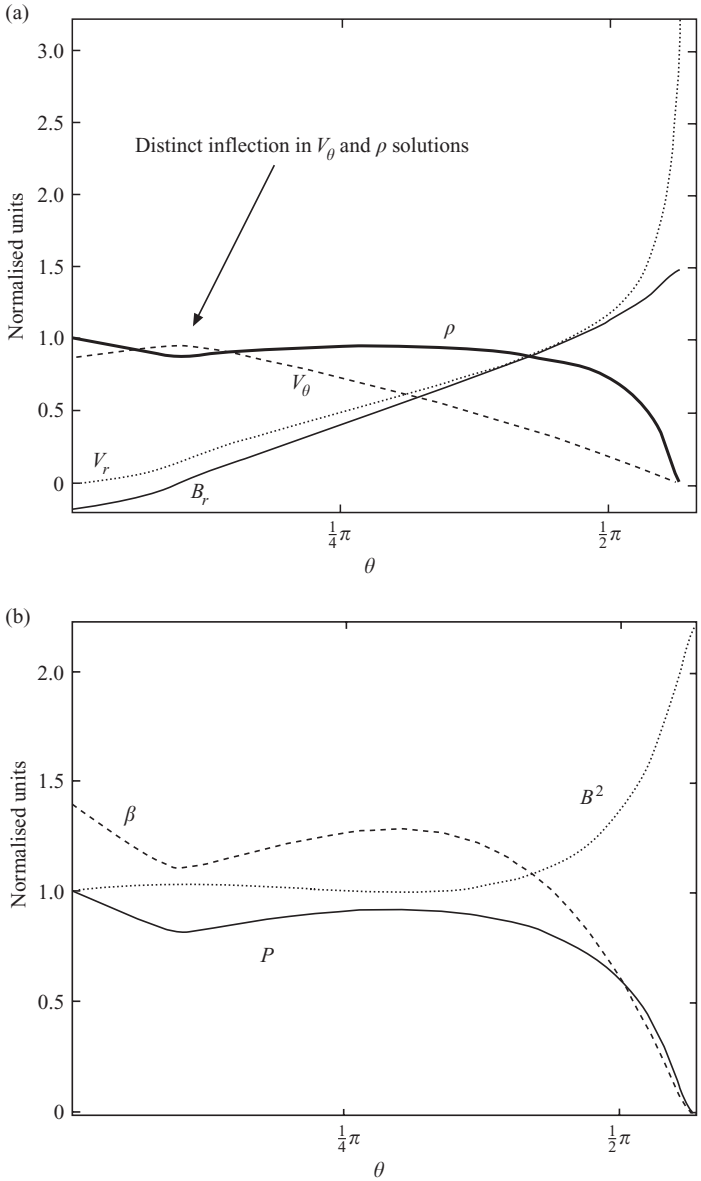

Figure 7. The structure of a slow-mode expansion wave when $\phi = 100°$ and $\frac{1}{2}\gamma\beta_0 = 1.4$. In (a), the thick solid, short dashed, long dashed and thin solid lines show the density, V_r, V_θ and B_r respectively as functions of θ. Note the density inflection point corresponding to the reversal in the direction of B_r. (b) shows the plasma pressure (solid line), magnetic pressure (short dashed line) and local plasma beta (long dashed line) as functions of θ.

$\phi = \frac{1}{2}\pi$ or $\frac{3}{2}\pi$, the flow and field are aligned, so that the slow mode only exists when $\frac{1}{2}\gamma\beta_0 < 1$, and then only compressive solutions exist.

As an example, Fig. 7(a) shows the density, V_r, V_θ and B_r for a case with $\phi = 100°$ and $\beta_0 = 1.4$, where the solution is plotted over all θ up to the vacuum condition. This differs in a number of ways from the fast-mode expansion wave. First, for a particular range of β_0, the solutions do not need to pass through a critical point

https://doi.org/10.1017/S0022377801001398 Published online by Cambridge University Press

to attain the vacuum condition. This range of β_0 is such that locally $\beta < 2/\gamma$ as B_r changes its sign, so $V_\theta = C$ (local sound speed), $\alpha \neq 1$, and there is no critical point. Secondly, the density does not decrease monotonically for all values of θ. There is a smooth inflection point at small θ that also corresponds to the location where $B_r = 0$.

To help understand this further, Fig. 7(b) shows the plasma and magnetic pressure and the local value of β as functions of θ. One important feature is the relative phase of the plasma and magnetic pressures. As would be expected for a slow-mode wave, they are out of phase at all locations. A second important point is that for all these cases we find that the local value of β decreases as one moves into the expansion wave. Thus, if $\frac{1}{2}\gamma\beta_0 > 1$, one might expect to encounter an umbilical point with $\beta = 2/\gamma$. As β_0 is increased, the inflection becomes more defined and we find that $M^2_{A\theta}$ approaches unity until, for a unique $\beta_0 = \beta_{\rm crit}$, $\frac{1}{2}\gamma\beta = 1$ at the inflection point, corresponding to an umbilic point. Clearly the inflection point plays a special role in the existence of this continuous solution – but in a less restrictive way than does the critical point in fast-mode expansion waves. The approach to the umbilic condition can be compared to the behaviour of a solar breeze solution (see e.g. Priest 1982), with the inflection becoming sharper, and tending towards a discontinuous gradient change at the umbilic point. So we again have $\beta_{\rm crit}$ corresponding to an umbilic critical solution, as in the fast case. However, unlike the fast-mode case, this solution is not unique for a particular ϕ, and we have continuous solutions for all β_0 in the range $\beta_0 \leqslant \beta_{\rm crit}$. For higher β_0 ($\beta_0 > \beta_{\rm crit}$), we find the solutions behaving in a similar manner to $\frac{1}{2}\gamma\beta_0 \leqslant 1$, but in this case, when B_r changes sign, $V_\theta = V_A$ and $M^2_{A\theta} = 1$. Thus there is a critical point for all solutions with $\beta_0 > \beta_{\rm crit}$, transition through which leads to attainment of vacuum conditions. As β_0 is further increased, we find that the solutions exist at increasing values of θ, and eventually become double-valued and unphysical when the vacuum condition is reached when $\theta > 2\pi$.

The solutions show a strong dependence on ϕ and β_0. Figures 8(a) and (b) summarise the properties when $\pi > \phi > \frac{1}{2}\pi$, with fig 8(a) and (b) showing $\beta_0 = 2$ and 0.2 respectively. The solid and dashed lines show B_r and ρ. For high β_0, the only permissible solution at $\phi = \frac{1}{2}\pi$ is a fast-mode wave. For high β_0 with ϕ fractionally greater than $\frac{1}{2}\pi$, we find that the solutions extend to create a very large fan, with the inflection point located at a large value of θ. These cases with ϕ close to $\frac{1}{2}\pi$ can also attain vacuum conditions when $\theta > 2\pi$, and hence are unphysical. As ϕ increases, the width of the expansion wave decreases, with the inflection point moving to lower values of θ, and becomes less pronounced when $\phi = 135°$. For low values of β_0 (Fig. 8b), the solutions do not have an inflection or umbilical point, since $\frac{1}{2}\gamma\beta_0 < 1$, and β decreases with θ. For $\beta_0 < 2/\gamma$, we find an overall smaller set of solutions (i.e. smaller termination θ). Finally, as ϕ approaches π, the density profile exhibits steep solutions near $\theta = 0$, and at $\theta = \pi$ there are no slow-mode solutions.

When $\pi < \phi < \frac{3}{2}\pi$, there are no slow-mode expansion waves for *any* value of $\frac{1}{2}\gamma\beta_0$. The flow always undergoes compression, as we found for the case with flow and field aligned, and eventually breaks down at a critical point. Figures 9(a) and (b) show examples of these solutions for $\beta_0 = 2$ and 0.2 respectively. The density increases monotonically up to a point where the solution breaks down, just as in the critical solutions found earlier. We have also demonstrated that the properties

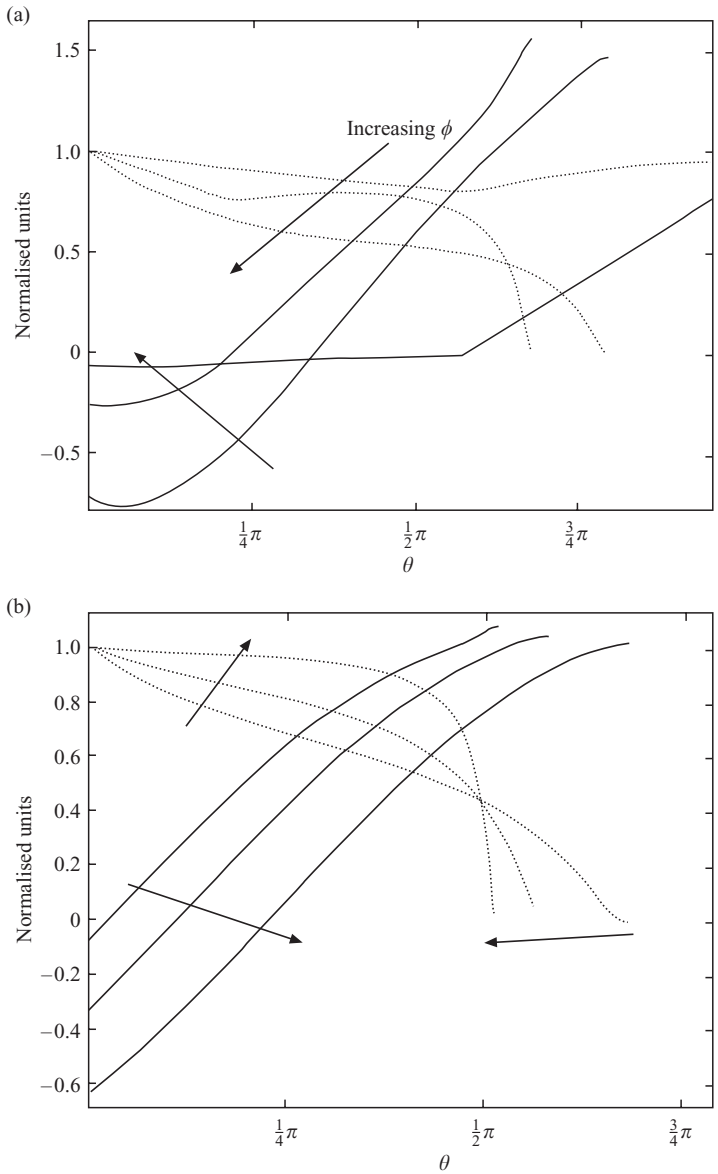

Figure 8. The structure of slow-mode expansion waves in the range $\frac{1}{2}\pi < \phi < \pi$. (a) shows the density (dashed lines) and B_r (solid lines) for $91^\circ < \phi < 135^\circ$, with $\beta_0 = 2$. Solutions with increasing values of ϕ are indicated by the arrows. Note the inflection point that moves to smaller θ as ϕ increases. (b) shows results for $\phi = 95^\circ$, 110° and 160°, for $\beta_0 = 0.2$. Note the absence of an inflection point.

when $0 < \phi < \frac{1}{2}\pi$ are the same as those with $\pi < \phi < \frac{3}{2}\pi$, and the same holds when $\frac{3}{2}\pi < \phi < 2\pi$ and $\frac{1}{2}\pi < \phi < \pi$.

4.4.1. Behaviour of slow-mode waves at critical values of ϕ. It is of particular interest to understand how the slow-wave properties change as the four critical angles (0, $\frac{1}{2}\pi$, π and $\frac{3}{2}\pi$) are crossed. Due to the 180° symmetry of the solutions, we concentrate

https://doi.org/10.1017/S0022377801001398 Published online by Cambridge University Press

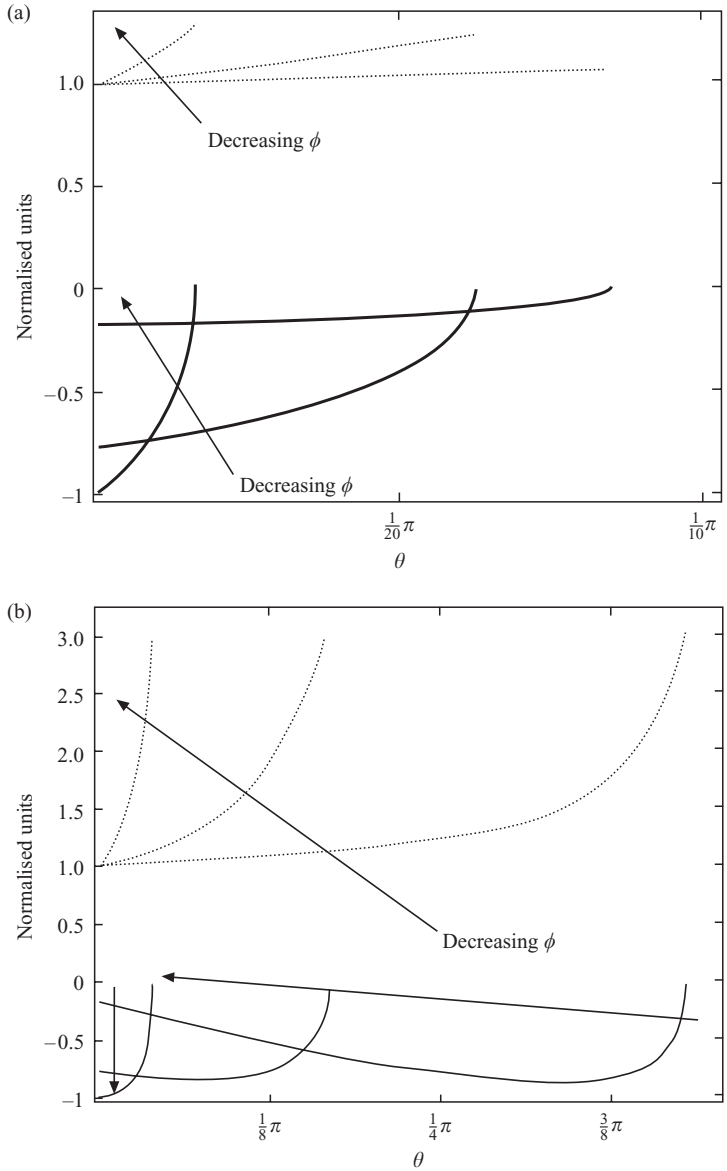

Figure 9. The structure of self-similar slow-mode waves in the range $\pi < \phi < \frac{3}{2}\pi$. Three values of ϕ are shown: 260°, 220° and 190°. (a) and (b) show $\beta_0 = 2$ and 0.2 respectively. In all cases, the waves are compressive and break down at a finite value of θ, with the breakdown taking place at smaller values of θ as ϕ decreases.

on $\phi = \frac{1}{2}\pi$ and π. The latter case is straightforward. As noted above, when $\phi = \pi$ is approached from below, the density gradient becomes increasingly negative near $\theta = 0$, resulting in an increasingly rapid attainment of vacuum conditions, until the solution vanishes completely at $\phi = \pi$. As ϕ approaches π from above, the solution breaks down (i.e. develops infinite gradients) at smaller values of θ, until at $\phi = \pi$ it does not exist. Thus only the fast-mode wave can exist at $\phi = \pi$.

The case of $\phi = \frac{1}{2}\pi$ is more complicated, and the results depend on the value of β_0.

https://doi.org/10.1017/S0022377801001398 Published online by Cambridge University Press

Table 1. Properties of the slow mode as a function of ϕ.

Range of ϕ	Slow-mode properties
$\phi = 0, \pi$	No slow-mode wave (all $\frac{1}{2}\gamma\beta_0$)
$\phi = \frac{1}{2}\pi, \frac{3}{2}\pi$	Slow-mode compressive wave if $\frac{1}{2}\gamma\beta_0 < 1$ (field and flow aligned) No slow mode if $\frac{1}{2}\gamma\beta_0 > 1$
$\frac{1}{2}\pi < \phi < \pi$, $\frac{3}{2}\pi < \phi < 2\pi$	Undergoes full expansion to vacuum conditions. Continuous solutions for $\frac{1}{2}\gamma\beta < 1$. Critical point for $\frac{1}{2}\gamma\beta > 1$ at $B_r = 0$, with umbilic solution at $\frac{1}{2}\beta = 1$. High β_0, ϕ near $\frac{1}{2}\pi$ attain unphysical $\theta > 2\pi$ solutions
$\pi < \phi < \frac{3}{2}\pi$, $0 < \phi < \frac{1}{2}\pi$	Permature termination at finite density (all $\frac{1}{2}\gamma\beta_0$). Compressive

For $\frac{1}{2}\gamma\beta_0 < 1$, we require that in the limit of $\phi \to \frac{1}{2}\pi$, the slow mode become purely compressive (see Sec. 4.2). For $\frac{1}{2}\gamma\beta_0 \ll 1$ and ϕ near $\frac{1}{2}\pi$, the density is approximately constant for the majority of the wave, and then abruptly decreases to achieve the vacuum condition. As we increase $\frac{1}{2}\gamma\beta_0$ towards unity, the density becomes more compressive, similar in appearance to the post-inflection density solution in the $\frac{1}{2}\gamma\beta_0 > 1$ case. For ϕ slightly less than $\frac{1}{2}\pi$, we find the density to be compressive and terminated by a breakdown of the solution. The overall behaviour about this point can be described as 'cusp-like' in that for ϕ just less than $\frac{1}{2}\pi$ we have the solution tending to very large values (gradient $\to +\infty$) and for ϕ just greater than $\frac{1}{2}\pi$, we have the solution $\to 0$ (gradient $\to -\infty$), with $\phi = \frac{1}{2}\pi$ corresponding to a finite-density, zero-angular-velocity fan termination.

For $\frac{1}{2}\gamma\beta_0 > 1$, ϕ approaches $\frac{1}{2}\pi$ from above, and the inflection point moves to larger values of θ, corresponding to a larger overall θ at termination. As mentioned previously, this also corresponds to double-valued unphysical solutions in θ. At $\phi = \frac{1}{2}\pi$, we have no solution, since we have a fast-mode wave only. Approaching $\frac{1}{2}\pi$ from below, solutions with density gradients $\to +\infty$ in very small θ exist. Thus, as we pass from high to low ϕ through $\phi = \frac{1}{2}\pi$, we find the large $\theta > 2\pi$ solutions, moving to no slow-mode solution at $\phi = \frac{1}{2}\pi$, to very small compressive solutions with gradients $\to +\infty$.

The results as a function of ϕ can be summarised as in Table 1.

5. Conclusions

This paper has presented a comprehensive range of solutions of the MHD equations corresponding to self-similar expansion (and compression) waves. The solutions have revealed a surprisingly complexity to this problem. There are serious restrictions in parameter space where solutions exist that ultimately attain a vacuum condition after a finite distance. Fast-mode expansion waves exist only for a single condition at the start of the expansion; slow-mode waves exist only for a range of angles between flow and field. In other cases, either the wave becomes compressive or the solution fails before reaching a vacuum condition.

The implications of this work for space physics are numerous. Two examples are the presence of expansion waves in the cusp and in the distant magnetotail. In the former case, the expansion is expected to be fast-mode, and is thus unlikely to occur in anything other than the high-beta limit, or for field-aligned flow. The result is then likely to be a very turbulent transition while the magnetosheath flow tries to

turn into the cusp, and cannot do so in a steady manner. In the latter case, one can expect the proposed expansion to depend crucially on the interplanetary magnetic field conditions. For some values, a smooth expansion if possible, but for others, only a compressional solution will exist. The implications to these situations will be discussed elsewhere.

Acknowledgement

M. Taylor acknowledges support from a UK PPARC studentship.

References

Cargill, P. J. 1999 A model for plasma flows and shocks in the high latitude cusp. *J. Geophys. Res.* **104**, 14 647.

Curle, N. and Davies, H. J. 1971 *Modern Fluid Dynamics*. New York: Van Nostrand Reinhold.

Goedbloed, J. P. and Lifschitz, A. 1997 Stationary symmetric MHD flows. *Phys. Plasmas* **4**, 3544.

Grad, H. 1960 Reducible problems in magneto-fluid dynamic steady flows. *Rev. Mod. Phys.* **32**, 830.

Krisko, P. H. and Hill, T. W. 1991 Two dimensional model of a slow mode expansion fan at Io. *Geophys. Res. Lett.* **18**, 1947.

Landau, L. D. and Lifschitz, E. M. 1988 *Fluid Dynamics*. Oxford: Pergamon.

Myong, R. S. 1997 Analytical results on MHD intermediate shocks. *Geophys. Res. Lett.* **22**, 2929.

Priest, E. R. 1982 *Solar Magnetohydrodynamics*. Dordrecht: Reidel.

Siscoe, G. L. and Sanchez, E. M. 1987 An MHD model for the complete open magnetotail boundary. *J. Geophys. Res.* **92**, 7405.

Siscoe, G. L., Lyon, E. F., Binsack, J. H. and Bridge, H. S. 1969 Experimental evidence for a detached lunar compression wake. *J. Geophys. Res.* **74**, 59.

Taylor, M. 2000 MHD modelling of space plasmas. PhD thesis, Imperial College, London.

Weber E. J. and Davis, L. 1967 The angular momentum of the solar wind. *Astrophys. J.* **148**, 217.